Implanted Neural Progenitor Cells Regulate Glial Reaction to Brain Injury and Establish Gap Junctions with Host Glial Cells

Rocío Talaverón, Esperanza R. Matarredona, Rosa R. de la Cruz, David Macías, Victoria Gálvez, and Angel M. Pastor

Transplantation of neural stem/progenitor cells (NPCs) in the lesioned brain is able to restore morphological and physiological alterations induced by different injuries. The local microenvironment created at the site of grafting and the communication between grafted and host cells are crucial in the beneficial effects attributed to the NPC implants. We have previously described that NPC transplantation in an animal model of central axotomy restores firing properties and synaptic coverage of lesioned neurons and modulates their trophic factor content. In this study, we aim to explore anatomical relationships between implanted NPCs and host glia that might account for the implant-induced neuroprotective effects. Postnatal rat subventricular zone NPCs were isolated and grafted in adult rats after transection of the medial longitudinal fascicle. Brains were removed and analyzed eight weeks later. Immunohistochemistry for different glial markers revealed that NPC-grafted animals displayed significantly greater microglial activation than animals that received only vehicle injections. Implanted NPCs were located in close apposition to activated microglia and reactive astrocytes. The gap junction protein connexin43 was present in NPCs and glial cells at the lesion site and was often found interposed within adjacent implanted and glial cells. Gap junctions were identified between implanted NPCs and host astrocytes and less frequently between NPCs and microglia. Our results show that implanted NPCs modulate the glial reaction to lesion and establish the possibility of communication through gap junctions between grafted and host glial cells which might be involved in the restorative effects of NPC implants.

Introduction

Neural stem/progenitor cells (NPCs) are a heterogeneous population of self-renewing and multipotent cells in the developing mammalian nervous system as well as in the subventricular zone (SVZ) of the lateral ventricles and the hippocampal dentate gyrus of the adult brain (Alvarez-Buylla et al., 2002; Anderson, 2001; Gage, 2000). NPCs can give rise to the three major lineages of the nervous system: neurons, astrocytes and oligodendrocytes and can be expanded *in vitro* from fetal, postnatal or adult brains (Carpenter et al., 1999; Gage, 2000; Reynolds and Weiss, 1992; Svendsen et al., 1996). In recent years, the use of NPCs for transplantation purposes has been tested in different types of nervous system

disorders such as Parkinson's disease, Huntington's disease, multiple sclerosis, spinal cord injury or stroke, with generally reported beneficial effects (Cummings et al., 2005; Kelly et al., 2004; McBride et al., 2004; Pluchino et al., 2003, 2005; Richardson et al., 2005; Ziv et al., 2006). The local microenvironment that surrounds implanted NPCs in the injured nervous system has been described to influence NPC survival, integration, migration and differentiation (Englund et al., 2002; Jeong et al., 2003; Pluchino et al., 2003, 2005; Pluchino and Cossetti, 2013; Yang et al., 2002) and, in turn, NPC-derived signaling factors also influence this local environment and can be partially responsible for the beneficial effects attributed to NPC implants (Mosher et al., 2012;

Talaverón et al., 2013). How signals from the endogenous micro-environment affect implanted NPCs and vice versa is a crucial question to understand the mechanisms underlying the benefits of transplanted cell-based therapies.

In line with this, Jäderstad et al. (2010) have recently described that communication via gap junctions between implanted NPCs and host neurons is an essential step in their integration into the host neural circuitry and in the mechanisms of their protective effects. Indeed, suppression of the gap-junctional intercellular communication is associated with significant decreases in the host rescue effects attributed to NPC engraftment (Jäderstad et al., 2010). Gap junctions allow the exchange of ions, second messengers and low weight molecules between connected cells, therefore providing a mechanism for the coordination of metabolic and electrical activities (Bruzzone et al., 1996; Kumar et al., 1996). A gap junction channel is formed by two joined hemichannels, each comprising six monomers of connexins, a family of proteins with more than 20 members (reviewed in Söhl and Willecke, 2003). Among all connexin isoforms, connexin43 (Cx43) is the predominant isoform within the CNS. Cx43 has an important role in the neurogenic process of NPC proliferation, differentiation and migration during development (Cheng et al., 2004; Duval et al., 2002; Elias et al., 2007; Marins et al., 2009; Santiago et al., 2010). In the postnatal and adult brain, Cx43 expression becomes much more restricted to astrocytes (Rash et al., 2001), but its expression remains in ependymal and endothelial cells, NPCs and migratory neuroblasts of the SVZ (Contreras et al., 2004; Lacar et al., 2011; Miragall et al., 1997; Nagy and Rash, 2000). Cx43 protein expression significantly changes in astrocytes following various models of CNS injury (Chew et al., 2010; Esen et al., 2007; Lee et al., 2005; Nakase et al., 2006). Interestingly, microglial cells, which do not express Cx43 under resting conditions, become immunoreactive to this connexin isoform after brain stab-wound injury (Eugenin et al., 2001) or in response to inflammatory stimuli such as cytokines or bacterial pathogens (Eugenin et al., 2001; Garg et al., 2005). Therefore, communication via gap junctions in glial cells may be important for tissue remodeling in a diseased state.

In previous reports, we have shown that implanted NPCs from the postnatal SVZ prevent the alterations in firing properties and synaptic coverage induced after the transection of the medial longitudinal fascicle (MLF) in the axotomized abducens internuclear neurons (Morado-Díaz et al., 2011), and also modulate their neurotrophic factor content (Talaverón et al., 2013). Now we have focused on the analysis of possible interactions between implanted NPCs and host glial cells that might be relevant not only for the

integration of implanted cells but also for the prevention of lesion-induced alterations. Therefore, we have explored the glial reaction to lesion and NPC implantation, as well as the possibility of gap junctional communication between implanted NPCs and activated host astrocytes and microglia, as a likely important pathway mediating the graft-host signaling finally leading to neuronal improvement.

Materials and Methods

Experiments were performed in adult and 7-day postnatal (P7) Wistar rats in accordance with the guidelines of the European Union (2010/63/EU) and Spanish law (R.D. 53/2013 BOE 34/11370-420, 2013) for the use and care of laboratory animals. Surgical procedures used in this study were approved by the ethics committee of Universidad de Sevilla.

Neural Progenitor Cell Culture and Transduction

Neural progenitor cells were isolated from the SVZ of P7 rats (Fig. 1A) and were expanded in the form of neurospheres as described before (Talaverón et al., 2013; Torroglosa et al., 2007) (Fig. 1B).

Neurospheres were transduced with a lentiviral vector containing a reporter gene encoding for the green fluorescent protein (GFP) under the control of the cytomegalovirus promoter (Macías et al., 2009) with a titer of 3×10^6 IFU/mL and a multiplicity of infection of 3. Neurosphere-derived cells were incubated for 8 h with virus-added medium in T25 flasks containing 250,000 cells. After 72 h, cells from neurospheres expressed GFP (Fig. 1C). Neither viability nor multipoteniality of neurosphere-derived cells were affected by the viral transduction (Talaverón et al., 2013).

For immunocytochemical purposes, neurospheres were left to settle for 4 h on coverslips pretreated with poly-ornithine (Sigma Aldrich, St. Louis, MO) and then fixed with paraformaldehyde (4% in 0.1 M phosphate buffer, for 10 min).

CNS Lesion: Transection of the Medial Longitudinal Fascicle

Under general anesthesia (4% chloral hydrate, 1 mL/100 g, i.p.), adult rats were placed on a stereotaxic frame and a window trephined in the occipital bone. A unilateral transection of the right MLF was performed with a 750-μm width microblade aimed with a 35-degree anterior angle at the following stereotaxic coordinates: 3.5 mm caudal to lambda, 0 mm lateral and 7.5 mm depth (Paxinos and Watson, 1997) (Fig. 1D). The MLF contains, among others, axons of abducens internuclear neurons that project to the contralateral oculomotor nucleus and its disruption causes severe morphophysiological alterations within this neuronal population (de la Cruz et al., 2000; Pastor et al., 2000).

Neural Progenitor Cell Implantation

Immediately after lesion, a suspension of 50,000 viable GFP-expressing neurosphere-derived cells was prepared in DMEM/F-12 (Invitrogen, Camarillo, CA) and 1 μL of the cell suspension was injected at the same coordinates as the lesion with a Hamilton microsyringe coupled to a glass capillary (Fig. 1D). This
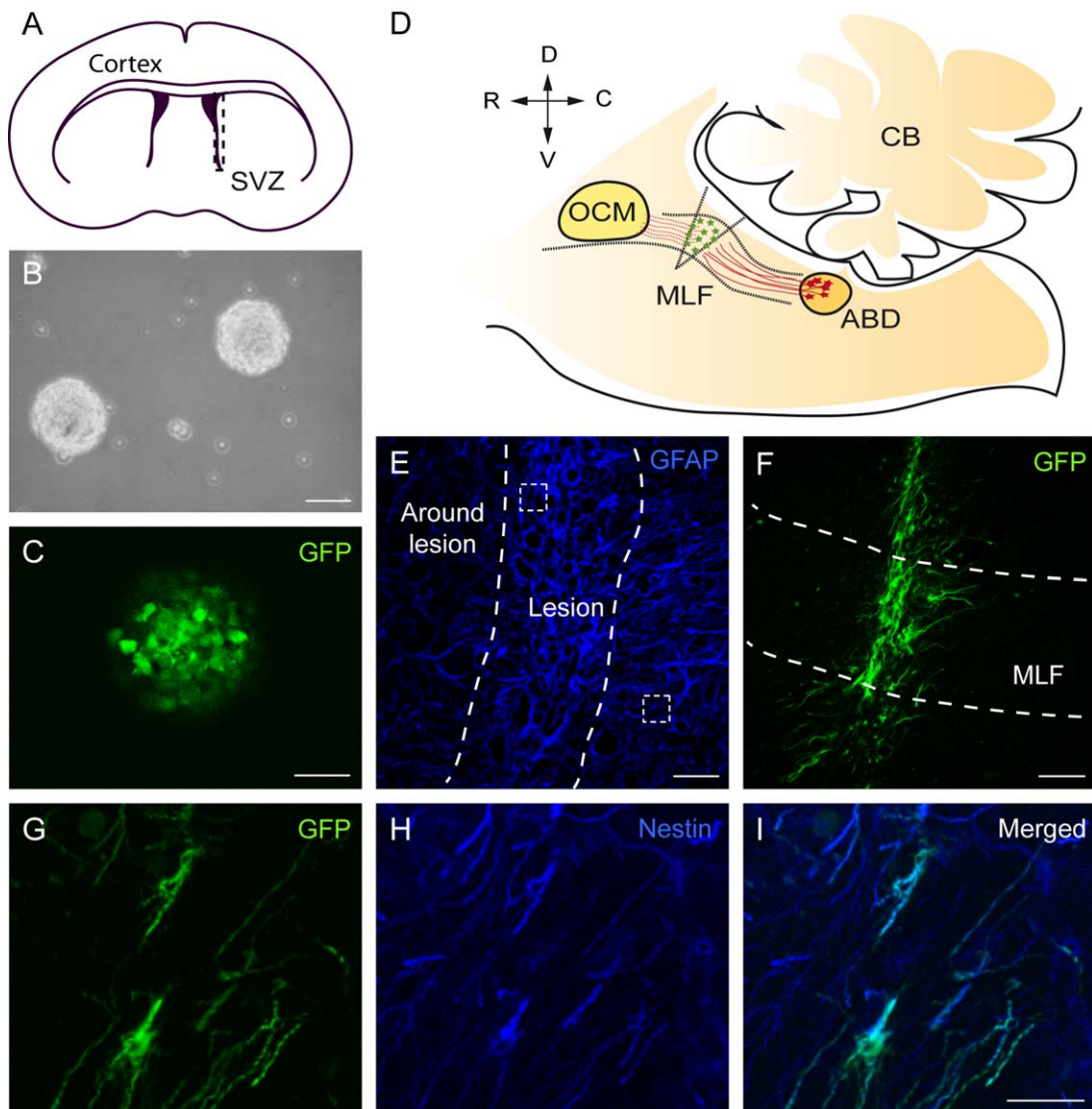
FIGURE 1: Neural progenitor cell culture, axotomy, cell implant and glial quantification. (A): Schematic drawing of a coronal slice obtained from a 7-day postnatal rat brain. Slices were cut beginning at the rostral opening of the third ventricle and extending 1.5-2.5 mm caudally. The subventricular zones (SVZ) adjacent to the lateral ventricles were dissected out (delimited between dashes) and neural progenitor cells contained in this region were cultured in the form of neurospheres. (B) and (C): Appearance of neurospheres in a phase contrast microscopy image (B) and in a confocal microscopy image showing GFP expression after viral transduction (C). Scale bar = 50 μm. (D): Schematic drawing of a rat brainstem parasagittal section showing the location of the medial longitudinal fascicle (MLF) transection and cell implant. Internuclear neurons of the abducens nucleus (ABD) are represented in red and implanted neural progenitor cells in green. Axons of abducens internuclear neurons (red lines) course through the MLF towards the contralateral oculomotor nucleus (OCM). The distal stumps of disrupted axons are represented in red dashed lines. (E): Confocal microscopy image from an axotomized rat brainstem section after GFAP immunohistochemistry (in blue). Lesion limits are represented between dashed lines and comprise approximately 75 μm bilaterally from the core of lesion. Examples of square boxes used to quantify optical density values of glial immunoreactivity in the lesion or around the lesion are shown. Scale bar = 50 μm. (F): Confocal microscopy image of a brainstem parasagittal section showing implanted cells identified by their GFP expression (in green) at the site of axotomy. Dorso-ventral limits of the MLF are shown in dashed lines. Scale bar = 100 μm. (G-I): Confocal microscopy images of a brainstem parasagittal section showing implanted cells identified by their GFP expression (in green, G) and after immunohistochemistry for nestin (in blue, H). I is the merged image of G and H. GFP- positive cell processes were immunoreactive for nestin. Scale bar = 25 μm. Dorso-ventral and rostro-caudal orientation of images D to I are the same as in D. Other abbreviations: C, caudal; CB, cerebellum; D, dorsal; GFAP, glial fibrillary acidic protein; GFP, green fluorescent protein; R, rostral; V, ventral. [Color figure can be viewed in the online issue, which is available at wileyonlinelibrary.com.]

experimental group will be referred to as implanted. Another group of animals, the so-called axotomized, received only vehicle injection (1 μL of DMEM/F-12) after the axotomy.

Eight weeks after lesion, animals were perfused transcardially under deep anesthesia (sodium pentobarbital, 50 mg/kg, i.p.) with 100 mL of physiological saline followed by 250 mL of 4%

paraformaldehyde in 0.1 M phosphate buffer, pH 7.4. Brainstems were removed and cryoprotected by immersion in a solution of 30% sucrose in sodium phosphate-buffered saline (PBS) until they sank. Then, 40-μm thick parasagittal sections were obtained with a cryostat to be processed for different immunostainings.

Immunohistochemistry for the Detection of Glial Cells and Connexin43

Parasagittal brainstem sections from axotomized and implanted animals were divided in adjacent series to be processed for the immunoidentification of astrocytes, oligodendrocyte precursors or activated microglia with antibodies raised against glial fibrillary acidic protein (GFAP), NG2 chondroitin sulfate proteoglycan (NG2), and MHC class II RT1B clone OX-6 (OX-6), respectively. After washing in PBS, sections were incubated with 1% sodium borohydride for 10 min for antigen retrieval. Sections were rinsed again in PBS and incubated for 1 h in a blocking solution consisting of 5% normal donkey serum in PBS with 0.1% Triton X-100 (PBS-T). Then, sections were incubated overnight at room temperature with one of the following primary antibodies: rabbit anti-GFAP (1:500; DAKO, Glostrup, Denmark, catalogue number Z0334), rabbit anti-NG2 (1:400; Millipore, Billerica, MA, catalogue number AB5320), mouse anti-MHC class II RT1B (Clone OX-6; 1:50; Serotec, Oxford, UK, catalogue number MCA46R) or goat anti-nestin (1:50; Santa Cruz Biotechnology, Dallas, TX, catalogue number sc-21249), prepared in blocking solution. After repetitive washings, sections were incubated for 2 h with the corresponding secondary antibody in PBS-T (anti-rabbit, anti-mouse or anti-goat IgG coupled to Cy3 or Cy5, 1:100; Jackson ImmunoResearch, West Grove, PA). Finally, sections were washed, mounted on slides and coverslipped with a 0.1 M solution of propyl gallate prepared in glycerol:PBS (9:1).

In some series of sections, immunohistochemistry for the detection of Cx43 (mouse anti-Cx43, 1:50, BD Biosciences, catalogue number 610062 or rabbit anti-Cx43, 1:200, Invitrogen, catalogue number 71-0700) was performed subsequently following the same described procedure but with the use of a biotinylated secondary antibody (biotinylated anti-mouse or anti-rabbit IgG, 1:500; Jackson ImmunoResearch) followed by 45-min incubation with DyLight 649 Streptavidin in PBS (1:800; Jackson ImmunoResearch).

Every immunohistochemical experiment was always performed simultaneously with sections from both axotomized and implanted animal groups.

Double immunocytochemistry for the simultaneous detection of nestin and Cx43 was performed in coverslips with attached neurospheres. Coverslips were incubated for 30 min in blocking solution containing 2.5% bovine serum albumin (BSA) in PBS and then overnight with the primary antibodies (goat anti-nestin from Santa Cruz Biotechnology at 1:50 and mouse anti-Cx43 from BD Biosciences at 1:50) and 1.5 h with the secondary antibodies (anti-goat and anti-mouse IgGs labeled with FITC and Cy5, respectively), all prepared in blocking solution. After repetitive washings, cells were counterstained with 4'-6'-diamidino-2-phenylindole (DAPI, 0.1 μg/mL) for 10 min. Finally, coverslips were mounted on slides with the mounting medium described before. Negative controls carried out by omission of the primary antibodies resulted in absence of staining in all cases.

Confocal Microscopy and Image Analysis

Images were captured with a confocal laser scanning microscope (Leica TCS SP2) using the 20×, 40×, and 63× objectives. Different focal planes separated 2 μm in the z-axis were scanned by exciting GFP, Cy3, and Cy5 fluorophores with excitation wavelengths of 488, 561, and 633 nm, respectively.

Quantification of GFAP-, NG2-, or OX-6-immunoreactivity was performed with Image J (NIH, Bethesda, MD) on 8-bit images captured with the 40× objective. Eight nonoverlapping square boxes of 30.4 μm (80 pixels) per side were randomly selected in the lesion site in the channel corresponding to the glial immunoreactivity image (Fig. 1E). Mean gray values (as an index of optical density, in counts per pixel) were obtained for every box and the average was calculated after background level substraction. The same procedure was performed in the same image in the region directly surrounding the lesion (a minimum lateral distance of 75 μm from the core of the lesion). Therefore, for every image, two optical density values were obtained, one in the lesion and other surrounding the lesion.

For the analysis of Cx43 expression by NPCs and glial cells, images (8-bit) were captured at different focal planes (0.5-1 μm along the z axis) with a Zeiss LSM DUO confocal microscope. GFP, Cy3 and DyLight649 fluorophores were excited with 488-nm argon, DPSS 561 nm and HeNe 633 nm lasers, respectively. For three-dimensional reconstructions, confocal Z-stacks were captured at 63× in 0.4 or 1 μm intervals and images rendered with the ZEN 2009 Light Edition software.

Fixation and Tissue Preparation for Electron Microscopy

Six implanted animals were prepared for electron microscopy processing. After a brief saline perfusion animals were fixed with 300 mL of 4% paraformaldehyde and 0.3% glutaraldehyde in phosphate buffer (PB) 0.1 M. Brains were cut in 50-μm thick parasagittal sections on a vibratome (Leica VT 1000 S). Sections were cryoprotected for 1 h by immersion in 25% sucrose and 10% glycerol in 0.05 M PB and then frozen and thawed three times on liquid nitrogen for membrane permeabilization. Finally, they were treated with 1% sodium borohydride in PB during 20 min and extensively rinsed in PB.

Double Pre-Embedding Immunohistochemistry

To analyse the anatomical relationships between implanted cells and host microglia, pre-embedding immunogold-silver detection of GFP (expressed by implanted cells) was combined with pre-embedding immunohistochemistry for the microglial marker Iba1 (ionized calcium binding adaptor molecule 1) using the avidin-biotin-peroxidase (ABC) method. In this procedure, sections were sequentially incubated in: (i) blocking solution, containing 0.2 M glycine, 0.2 M lysine, 0.2% BSA, and 10% normal goat serum (NGS) in PB, for 60 min; (ii) monoclonal mouse anti-GFP antibody (1:2,000; Millipore, catalogue number MAB3580) together with rabbit anti-Iba1 (1:1,000; Wako, Osaka, Japan, catalogue number 019–19741) diluted in 0.8% BSA and 5% NGS (incubation solution) for 48 h at 4°C; (iii) 1 nm colloidal gold-labeled goat anti-mouse IgG (Aurion, Wageningen, The Netherlands) diluted 1:100 together with biotinylated goat anti-rabbit IgG diluted 1:200 (Jackson

ImmunoResearch) prepared in incubation solution for 2 h at 20°C followed by 24 h at 4°C; (iv) 2% glutaraldehyde in PB for 10 min to fix gold particles. After each step, sections were rinsed (3 x 10 min) in PB. Gold particles were enlarged using silver enhancer (R-Gent SE-LM; Aurion) for 18 min at 20°C. The reaction was stopped in 0.03 M sodium thiosulphate (Aurion) for 10 min. Finally, sections were incubated in ABC (1:200; Vector Laboratories, Burlingame, CA) for 2 h at 20°C. The peroxidase reaction was developed using 0.05% 3,3'-diaminobenzidine tetrahydrochloride (DAB) (Sigma Aldrich) and 0.0075% hydrogen peroxide in PB for 5 min at 20°C. Afterwards, sections were washed and then postfixed with 1% osmium tetroxide in PB for 60 min at 20°C, stained in block with uranyl acetate for 45 min at 20°C, dehydrated through increasing graded ethanol series and flat-embedded in Durcupan resin (ACM; Fluka, Buchs, Switzerland).

In other sections, pre-embedding immunohistochemistry of GFP using the ABC method was combined with pre-embedding immunogold-silver detection of Cx43. Sections were incubated with rabbit anti-Cx43 (1:200; Invitrogen) and mouse anti-GFP (1:2000; Millipore) antibodies followed by 1 nm colloidal gold-labeled goat anti-rabbit IgG (1:100; Aurion; 1:100) and biotinylated goat anti-mouse IgG (1:500; Jackson ImmunoResearch). All steps were performed as described before.

Finally, ultrathin sections 60 nm thick were cut with an ultramicrotome (Leica EM UC7), collected on single-slot Formvar-coated nickel grids, counterstained with uranyl acetate and lead citrate and examined on a Philips CM-10 transmission electron microscope. Images were digitally captured using a VELETA side-mounted camera (Olympus).

Postembedding Immunohistochemistry of Glial Fibrillary Acidic Protein

Postembedding GFAP immunostaining was performed on ultrathin sections with an anti-GFAP antibody (rabbit, 1:500; DAKO) and a 5 nm colloidal gold-labeled goat anti-rabbit IgG (1:15; Sigma Aldrich) following an already reported procedure (Pastor et al., 2000). A silver enhancer method was applied to enlarge the size of the gold particles previous to counterstaining with lead citrate and uranyl acetate (Danscher and Zimmer, 1978).

Statistics

The optical density values of GFAP, NG2, and OX-6 immunofluorescence were compared between experimental groups (axotomized *vs.* implanted) and between locations (lesion *vs.* around lesion). The statistical analysis was carried out in Sigma Plot 11 (Systat Software) by using the two-way ANOVA followed by *post hoc* multiple comparisons (Holm-Sidak's method) at a significant level of $P < 0.05$. All values are expressed as the mean ± standard error of the mean (SEM).

Results

Local Glial Cell Response to Axotomy and NPC Implants

The glial reaction to axotomy and NPC implants was analyzed 8 weeks after injury. Implanted NPCs were identified in the host tissue by their GFP expression. They appeared dis-

tributed in areas restricted to the lesion site, approximately 75 μm lateral from the core of lesion in the rostrocaudal axis, and covering the dorsoventral limits of the MLF (Fig. 1F). Most of the implanted NPCs presented cell processes of variable length (15–50 μm for short processes and up to 200 μm for longer processes) and were immunopositive for nestin, an intermediate filament protein expressed by neural stem cells (Fig. 1G–I).

Quantification of the glial cell response to injury was carried out by comparing the intensity of immunofluorescence corresponding to each glial marker (i.e., optical density) in the lesion site with respect to that found in the surrounding tissue, as described in Materials and methods, based on a previously described procedure (Whitman et al., 2009).

Axotomy induced a significant sixfold increase in GFAP optical density in the lesion site as compared to the area around lesion (Fig. 2A,C). A similar astrocytic response to injury was obtained in implanted animals (Fig. 2B,C). No significant differences were found in GFAP optical density values between axotomized and implanted groups, therefore, the presence of NPCs at the site of injury did not quantitatively modify the astroglial reaction to the fascicle transection.

NG2-immunopositive cells presented oval cell bodies with multiple branched thin processes (inset in Fig. 2D). Analysis of NG2 immunoreactivity revealed that 8 weeks after MLF transection, optical density values remained similar in the lesion site as compared to the surrounding area (Fig. 2D,F), and this was applicable to implanted animals (Fig. 2E,F). Similarly, comparisons between experimental groups (i.e., axotomized *vs.* implanted) revealed no significant differences of immunofluorescence intensity using the oligodendrocyte precursor marker NG2 (Fig. 2F).

With respect to microglia, two major types of OX-6-positive (MHC-II expressing) cell morphologies were observed: microglial cells with short thick processes and further activation states characterized by ameboid morphology (Fig. 2G,I). The lesion site displayed significantly higher optical density values of OX-6 immunoreactivity than the surrounding area both for axotomized and implanted animals (Fig. 2G–I). However, OX-6 optical density within the lesion resulted in approximately two times more prominent values in NPC implanted animals than in animals that received only vehicle injections ($P < 0.05$; Fig. 2G–I).

Implanted NPCs are Located in Close Proximity to Reactive Astrocytes and Activated Microglia

GFAP immunohistochemistry in the lesion site of implanted animals revealed a close apposition between astrocytic processes and implanted cells (Fig. 3A–D). Frequently, we observed astrocytic processes surrounding a large portion of the cell body of GFP-positive cells (see arrows in Fig. 3A,B).
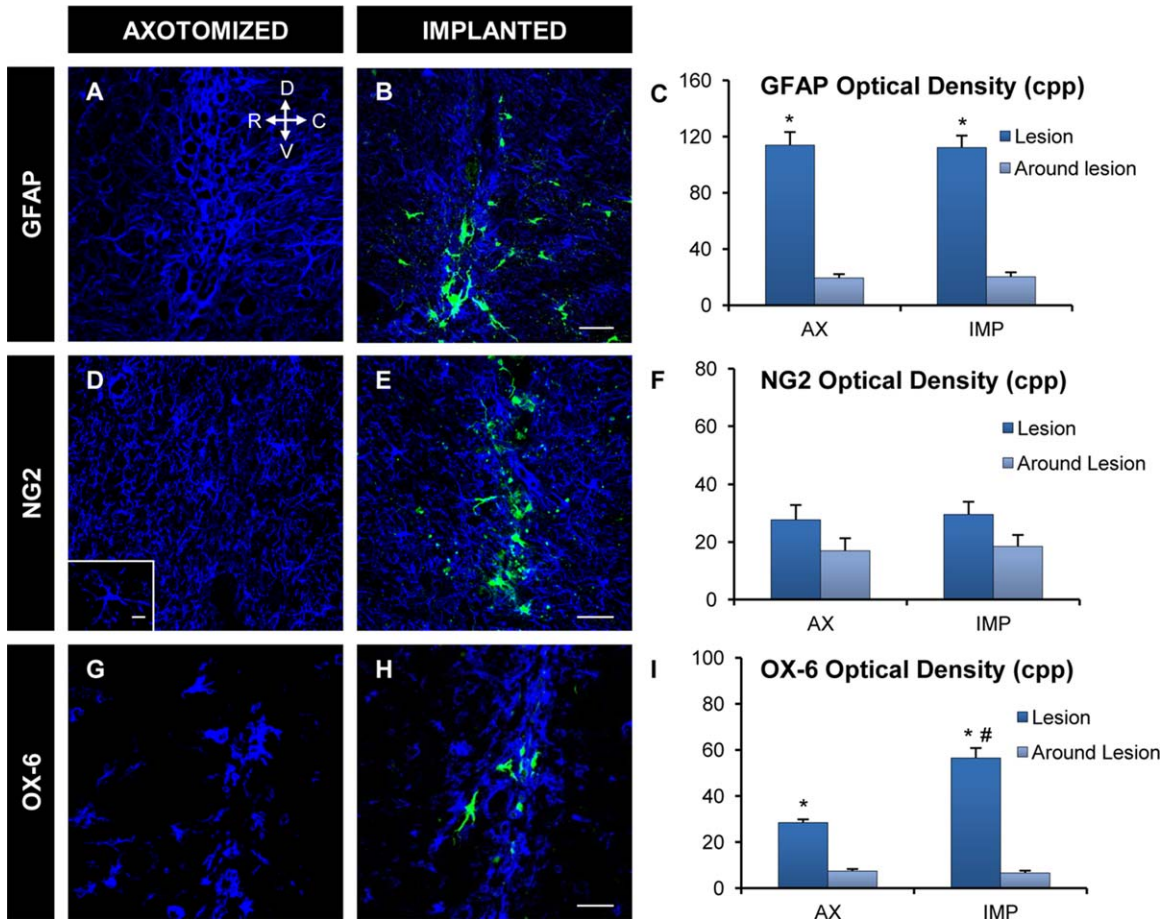
FIGURE 2: Glial reaction to axotomy and NPC implant. (A and B, D and E, G and H): Confocal microscopy images captured with the ×40 objective showing immunoreactivity to the astrocytic marker GFAP (A and B, in blue), the oligodendrocyte precursor marker NG2 (D and E, in blue) and the activated microglia marker OX-6 (G and H, in blue) in parasagittal sections containing the site of lesion from axotomized animals (A, D, G) and implanted animals (B, E, H). Implanted NPCs were identified in green by their GFP expression (B, E, and H; merged images of the glial marker and GFP channels). Inset in D represents a NG2-positive cell shown at higher magnification. Scale bars = 50 μm; 10 μm for the inset. C, caudal; D, dorsal; R, rostral; V, ventral. (C): Optical density values of GFAP immunoreactivity (in counts per pixel, cpp) in the lesion and around lesion from axotomized (AX) or implanted (IMP) animals. Bars represent the mean ± SEM of 8–10 sections analyzed from three different animals of each group. *$P < 0.05$, lesion compared to around lesion values. No significant differences between the axotomized and the implanted groups were found. (F): Optical density values of NG2 immunoreactivity (in counts per pixel, cpp) in the lesion and around lesion obtained from axotomized (AX) or implanted (IMP) animals. Bars represent the mean ± SEM of 8–9 sections analyzed from three different animals of each group. No significant differences were found between either lesion *versus* around lesion values in each group or axotomized *versus* implanted groups. (I): Optical density values of OX-6 immunoreactivity (in counts per pixel, cpp) in the lesion and around lesion from axotomized (AX) or implanted (IMP) animals. Bars represent the mean ± SEM of 28–31 sections analyzed from four different animals of each group. *$P < 0.05$, lesion compared to around lesion values; #$P < 0.05$, implanted compared to axotomized group. In C, F and I, the two-way ANOVA test was used followed by Holm-Sidak's method for multiple pairwise comparisons. [Color figure can be viewed in the online issue, which is available at wileyonlinelibrary.com.]

In addition, implanted NPCs were often located close to blood vessels together with astrocyte processes (Fig. 3C,D).

Some implanted NPCs developed long processes (up to 200 μm) directed mainly towards the caudal direction (Fig. 3E). Many of these cell processes were located in close proximity to activated microglial cells (Fig. 3E,G,H) and occasionally enwrapped them (Fig. 3E,F). In contrast, no evidence of close proximity between NG2-positive cells and NPCs was found.

Electron microscopy was performed to further confirm the interactions between implanted cells and host glia.

Implanted NPCs were identified at the ultrastructural level by pre-embedding GFP immunostaining (Fig. 4A,B). They presented a branched morphology with elongations arising from the cell body. Numerous astrocytes were visualized in the lesion site after postembedding immunogold staining for GFAP. Gold particles were associated specifically with their typical intermediate filaments (Fig. 4C,D). Pre-embedding immunostaining for Iba1 allowed the ultrastructural identification of microglial cells (Fig. 4E,F). They were characterized by their small size, irregular nucleus and clumps of nuclear chromatin, especially close to the
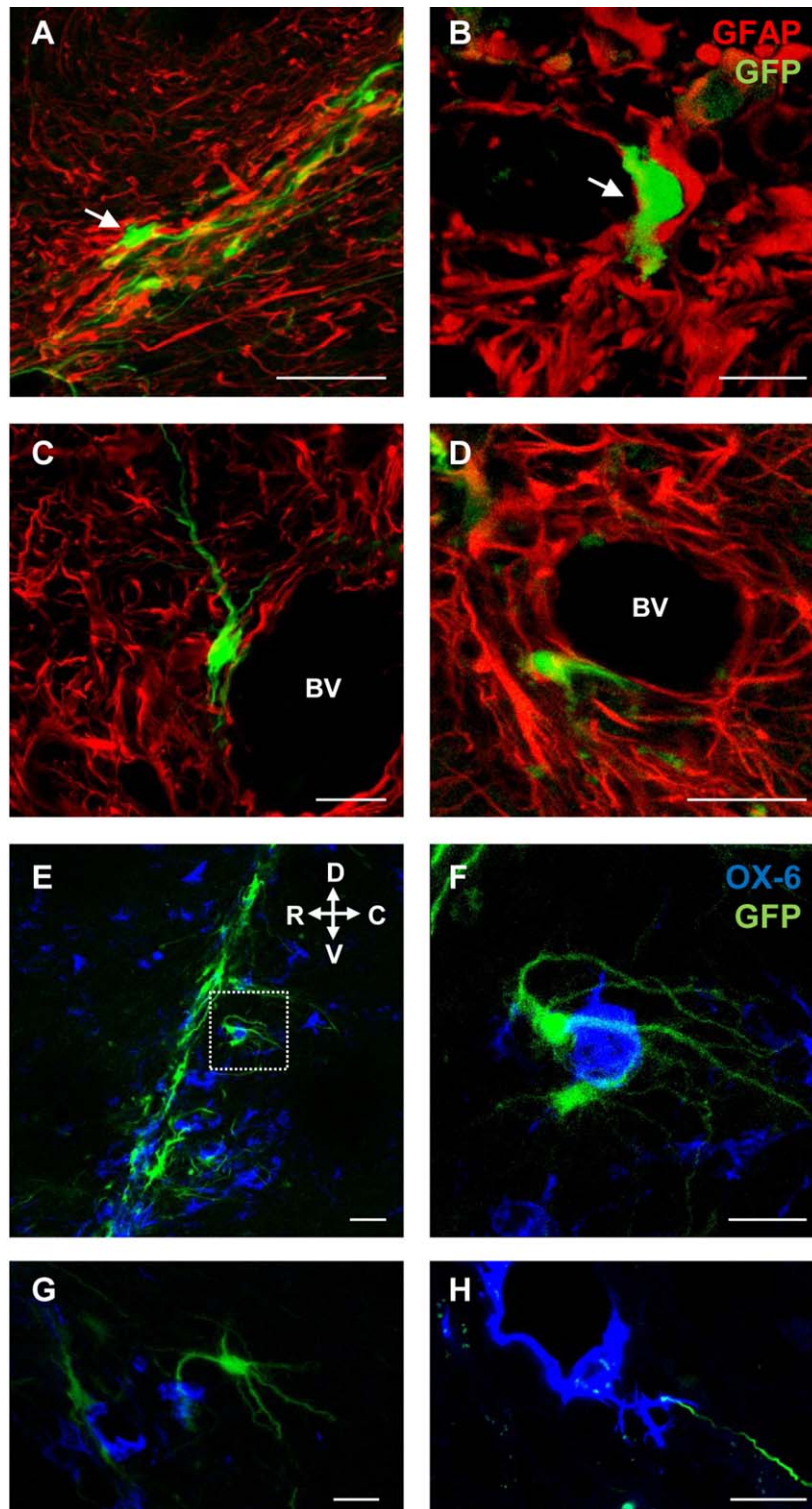
FIGURE 3: Close association between implanted NPCs and host glia. (A–D): Confocal microscopy images of parasagittal sections of the lesion site showing examples of the close proximity between implanted NPCs (GFP positive, in green) and reactive astrocytes (GFAP immunoreactive, in red). Arrows in A and B point to implanted cells surrounded by GFAP-positive processes. C and D are examples of implanted NPCs located nearby putative blood vessels (BV). Note that blood vessels appear surrounded by astrocytic processes. Scale bars = 50 μm in A and 25 μm in B to D. (E–H): Confocal microscopy images of parasagittal sections through the lesion site illustrating the close proximity between implanted NPCs (GFP-positive, in green) and activated microglia (OX-6 immunoreactive, in blue). F shows the framed region of E at higher magnification. Note NPC processes surrounding ameboid microglial cells. G and H illustrate processes of implanted cells adjacent to activated microglia. Scale bars = 50 μm in E and 25 μm in F to H. [Color figure can be viewed in the online issue, which is available at wileyonlinelibrary.com.]
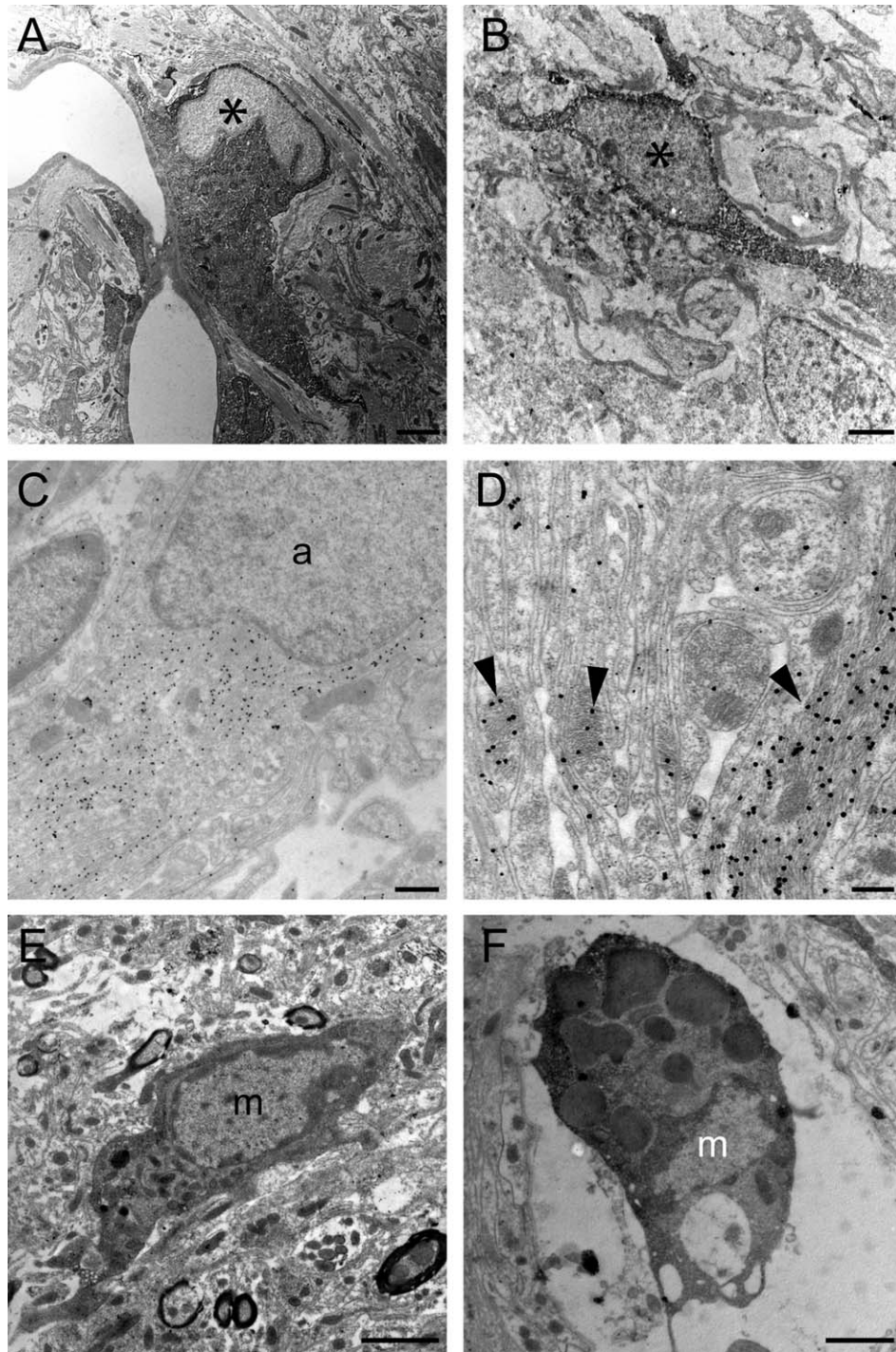
FIGURE 4: Ultrastructural and immunohistochemical identification of implanted NPCs and glial cells at the lesion site. (A, B): Examples of two NPCs identified by pre-embedding GFP immunohistochemistry using DAB, thereby conferring an electron-dense appearance to the cell (asterisks indicate the nucleus of the two NPCs). These cells presented a branched morphology (note the elongations arising from the implanted cell in B) and frequently appeared surrounded by a field of labeled processes (in A and B), that corresponded to either the observed cell or other neighboring implanted NPCs. The lesion site was characterized by a widened extracellular space (clearly notorious in B). Scale bars = 1 μm. (C, D): Electron microscopy images of astrocytes identified by post-embedding immunogold for GFAP. Note that gold particles are associated to filaments (arrowheads in D). The nucleus of the astrocyte in C is indicated as a. Scale bars = C, 0.125 μm; D, 0.5 μm. (E, F): Examples of two different types of microglial cells found at the lesion site according to their ultrastructural characteristics. Both types of microglia cells were identified by pre-embedding Iba-1 immunohistochemistry (DAB labeling). Note that the microglia in F is characterized by the presence of phagocytic vacuoles filling a large portion of its cytoplasm (ameboid type), whereas the microglia cell in E lacked such vacuoles. The nucleus of the microglia (m) typically contained clumped chromatin, specially surrounding the nuclear membrane. Scale bars = 2 μm.
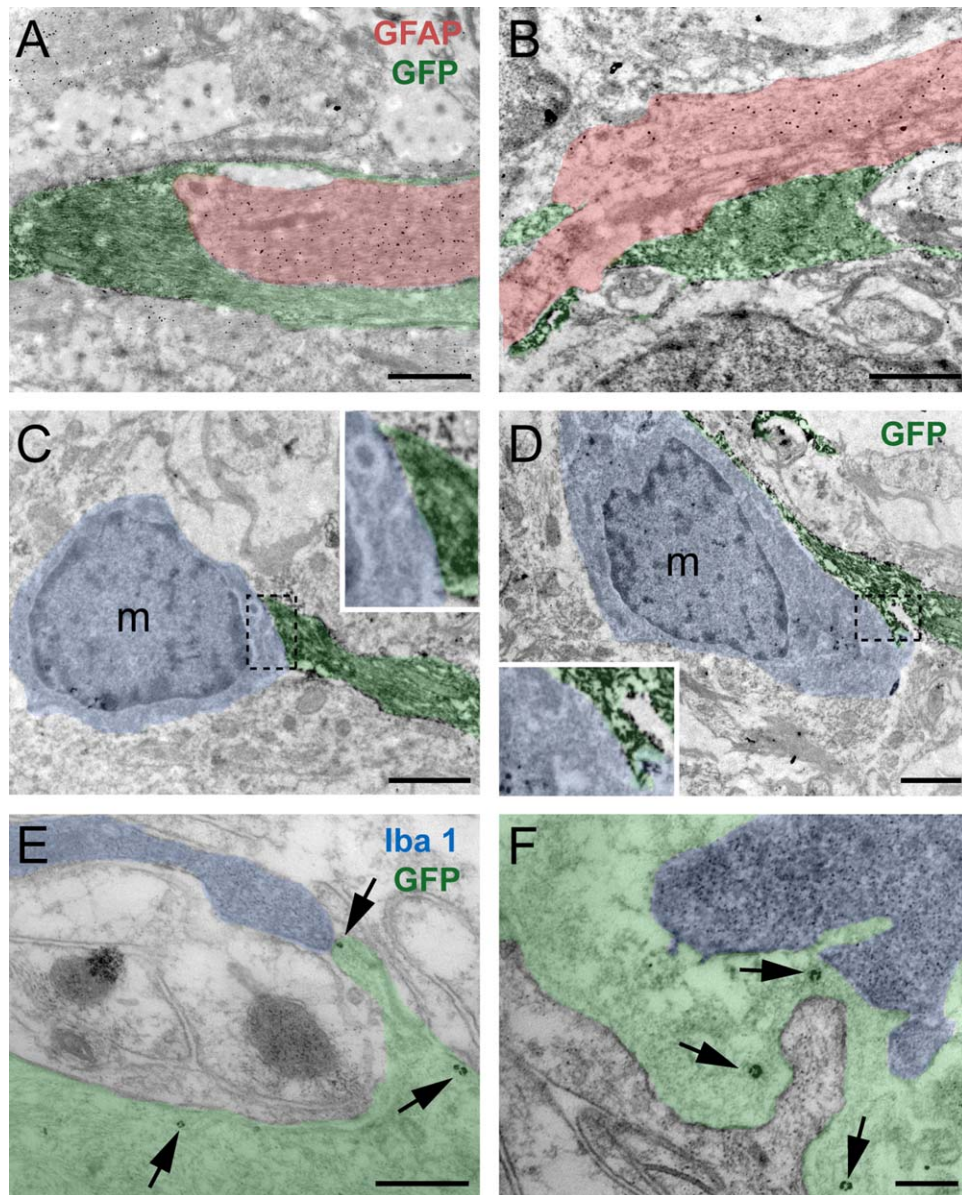
FIGURE 5: Direct appositions between implanted NPCs and glial cells at the lesion site. (A, B): Electron microscopy images of NPC processes identified by pre-embedding GFP immunohistochemistry with DAB (pseudo-colored in green) in direct contact to astrocytic prolongations labeled by GFAP immunogold (pseudo-colored in pink). Note the NPC process in A partly enwrapping an astrocytic element. Scale bars = A, 2 μm; B, 1.5 μm. (C, D): Direct contacts between the cell membranes of implanted NPCs (GFP-identified in pre-embedding with DAB; pseudo-colored in green) and likely microglial cells according to their ultrastructural features (pseudo-colored in blue; m indicates the microglial nuclei). Insets show higher magnification images of the framed regions in C and D to better illustrate the cell-to-cell contact. In some cases (D) an extensive area of the microglial plasma membrane appeared covered by NPC elements. Scale bars = 2 μm. (E, F): Examples of direct membrane appositions between identified NPC processes (labeled with GFP immunogold in pre-embedding; arrows point to some gold particles; pseudo-colored in green) and microglial elements (labeled with pre-embedding Iba1 immunocytochemistry using DAB; pseudo-colored in blue). Scale bars = 0.2 μm. [Color figure can be viewed in the online issue, which is available at wileyonlinelibrary.com.]

nuclear envelope (Fig. 4E,F; m). As previously observed at the confocal level, some microglial cells displayed ameboid appearance and contained phagocytic vesicles (Fig. 4F), whereas others lacked this phagocytic aspect (Fig. 4E).

At the ultrastructural level, we frequently observed direct appositions between GFP-immunostained NPC processes and GFAP-identified astrocytic profiles (Fig. 5A,B).

Direct contacts between labeled NPC processes and putative microglia were also detected (Fig. 5C,D; see also insets). In addition, it was also possible to observe direct appositions between NPCs and microglial cells, both identified, by combining GFP pre-embedding immunogold to identify the NPCs with Iba1 pre-embedding immunocytochemistry using DAB for the microglial identification (Fig. 5E,F).
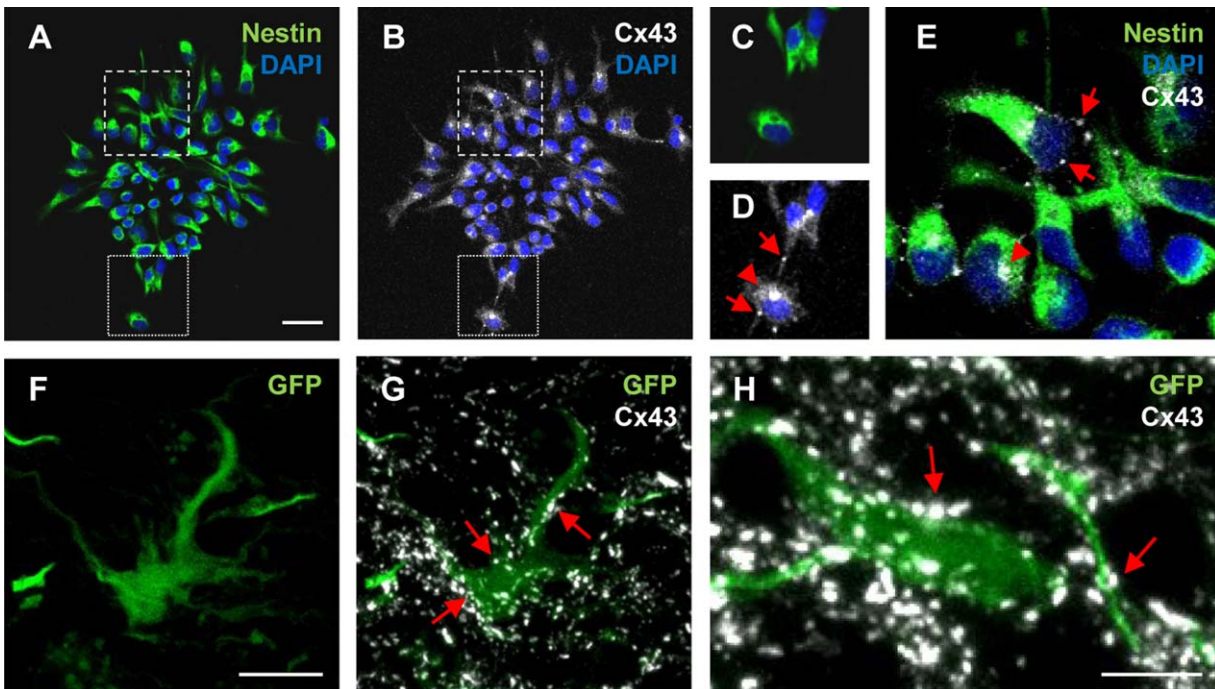
FIGURE 6: Cx43 expression in NPCs *in vitro* and after implantation. (A and B): Confocal microscopy images of a SVZ-derived neurosphere after double immunostaining for nestin (A, in green) and Cx43 (B, in white). Cell nuclei were identified by staining with DAPI (A and B, in blue). Scale bar = 25 μm. (C and D): Higher magnification images of the dotted frames of A and B, respectively. In D (also applies to E), red arrows point to Cx43-immunoreactive clusters showing a punctate appearance, whereas red arrowheads indicate other regions of the cell where Cx43-immunoreactive dots were evenly distributed. (E): Higher magnification image of the dashed frames in A and B showing the merged picture of the three channels corresponding to DAPI (blue) and immunoreactivity to nestin (green) and Cx43 (white). (F and G): Confocal microscopy images of an implanted cell identified by its GFP expression (F, green) showing Cx43 immunoreactivity (G, white) in the soma and in cell processes (examples in red arrows). Scale bar = 10 μm. (H): Higher magnification image showing the pattern of Cx43 immunoreactivity (in white) over a GFP-positive implanted cell (in green). The arrows point to some examples of Cx43-immunoreactive clusters characterized by their dotted aspect. Scale bar = 5 μm. [Color figure can be viewed in the online issue, which is available at wileyonlinelibrary.com.]

Gap Junction Protein Cx43 is Expressed by NPCs In Vitro and After Implantation in the Lesioned Tissue

The close apposition between the plasma membranes of implanted NPCs and host astrocytes and microglia led us to investigate the expression of the gap junction protein Cx43 in these cells to check for the possibility of gap junctions between them.

First, we wanted to elucidate whether Cx43 was already present in neurosphere-derived cells before their implantation. Double immunocytochemistry experiments for nestin and Cx43 revealed that most cells in each neurosphere were immunoreactive to nestin (98.9 ± 0.6%, Fig. 6A) and also to Cx43 (93.8 ± 1.7%; Fig. 6B, n = 892 cells from three different cultures). Indeed, most of the nestin-positive cells also presented Cx43 immunoreactivity (94.9 ± 0.4%; Fig. 6C–E).

In a further step, we determined whether Cx43 was also present in NPCs implanted at the lesioned MLF. Thus, 8 weeks after NPC implantation, Cx43 expression persisted in most of the GFP-positive implanted cells (77.12% of 153 analyzed cells). An example of an implanted GFP-identifed NPC is shown in Fig. 6F, which also revealed an intense labeling of Cx43-immunoreactive dots (Fig. 6G). Cx43 immunoreactivity in implanted cells was characterized by the presence of numerous labeled dots conferring a punctate appearance to this staining (Fig. 6G,H; arrows). Cx43-immunoreactive clusters were located over both the cell body and processes of implanted cells (Fig. 6G,H).

Identification of Cx43-Positive Profiles Located Between Implanted NPCs and Host Glial Cells

Reactive astrocytes at the lesion site also expressed Cx43 (Fig. 7A). Interestingly, Cx43-immunopositive clusters were often located at the intersection between NPCs and astrocytes. Some examples of Cx43-immunoreactive dots located between a GFAP-positive (astrocytic) and a GFP-positive (NPC) element are illustrated in Fig. 7B–E (circles).

Activated microglial cells (immunopositive for OX-6) located close to implanted NPCs also showed Cx43 immunoreactivity (Fig. 7F–H). Although less abundant than in astrocytes, interposition of Cx43-positive profiles between NPCs and microglial processes were also found. Some examples of these triads (microglia-connexin-implanted cell) identified by their respective markers (OX-6/Cx43/GFP) are outlined in the circles of Fig. 7I,J, and illustrated at a higher
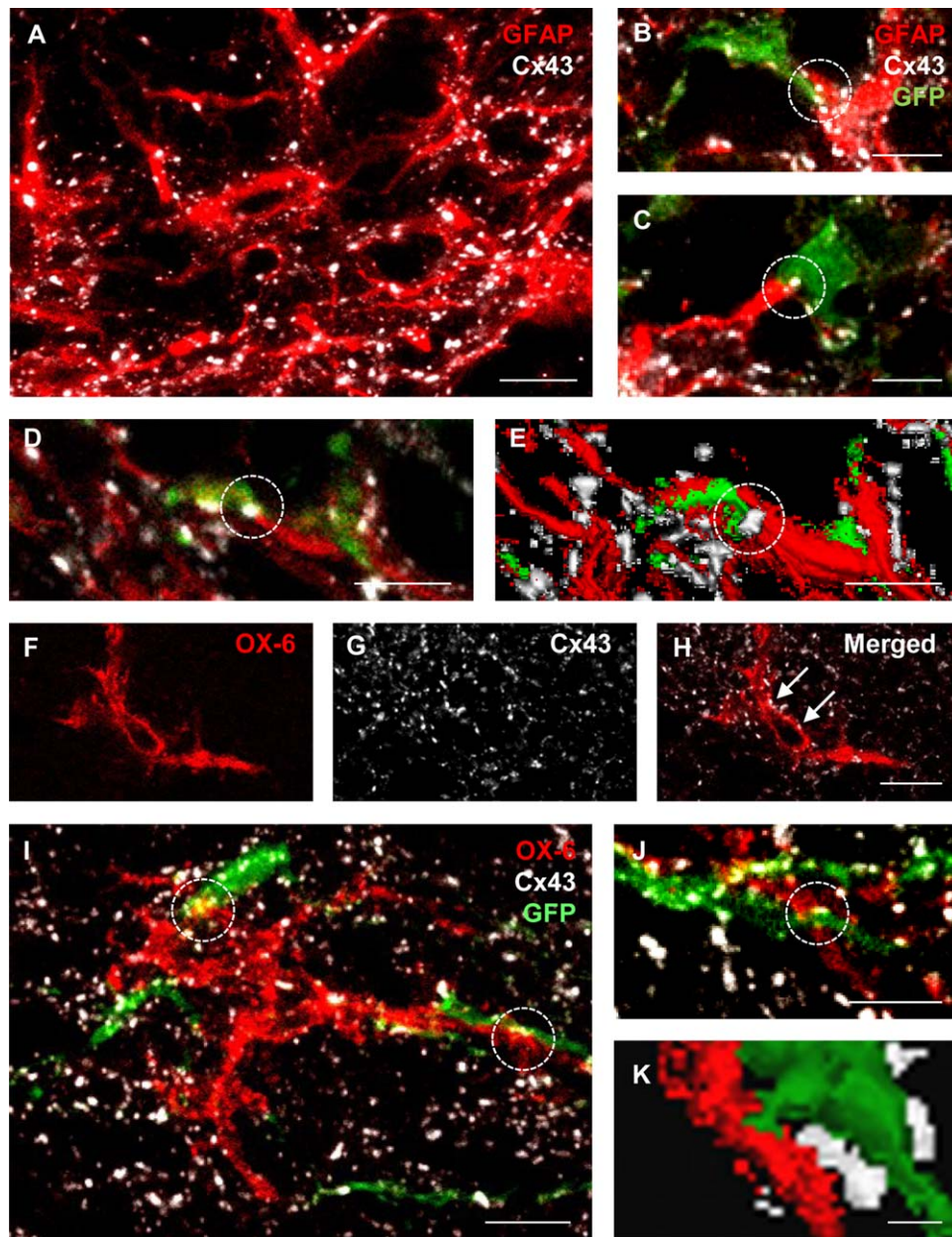
FIGURE 7: Cx43 expression in reactive astrocytes and activated microglia at the lesion site. (A): Confocal microscopy image showing Cx43-immunoreactive clusters (in white) on reactive astrocytes (GFAP-immunopositive, in red). Scale bar = 10 μm. (B–D): Confocal microscopy images of brainstem sections from implanted animals at the lesion site after double immunofluorescence for GFAP (in red) and Cx43 (in white) showing examples (delimited by dashed circles) of Cx43 location between implanted cells (GFP expression, in green) and astrocytic processes. Scale bars = 5 μm. (E): 3D reconstruction of one Z-stack formed by 5 confocal planes of 1 μm thickness, one of which is shown in D. Note Cx43-immunopositive clusters located between the process of one NPC and an astrocyte (dashed circle), suggesting the presence of gap junctions between these two cell types. Scale bar = 5 μm. (F–H): Confocal microscopy images of an activated microglial cell through the lesioned MLF (F, immunopositive for OX-6, in red) showing Cx43 expression (G, in white). Arrows in the merged image (H) point to some Cx43-immunoreactive dots over the microglial cell. Scale bar = 10 μm. (I and J): Confocal microscopy images obtained at the lesion site showing an OX-6-immunopositive microglial cell (in red), NPC processes (GFP-positive, in green) and Cx43-immunoreactive clusters (in white). Dashed circles delimite regions where Cx43-immunoreactive profiles appeared located between a microglial cell and a NPC process. Scale bars = 5 μm. (K): Three-dimensional reconstruction of one Z-stack made from six confocal planes of 1 μm thickness, captured from a brainstem section at the lesion site showing the tripartite configuration formed by a Cx43-immunoreactivity profile (white) located between a GFP-positive implanted NPC process (green) and an activated microglial process (OX-6-positive, red), suggestive of gap junctions formed between implanted cells and host microglia. Scale bar = 1 μm. [Color figure can be viewed in the online issue, which is available at wileyonlinelibrary.com.]

magnification in a rendered image in Fig. 7K. These findings indicate the possibility of communication between grafted NPCs and host astrocytes and microglia via gap junctions.

Ultrastructural Evidence of Gap Junctions in Implanted NPCs, Astrocytes, and Microglia at the Lesion Site

The combination of electron microscopy with immunohistochemistry against Cx43 by pre-embedding immunogold allowed us the ultrastructural demonstration of the presence of this connexin in gap junctions between cells at the lesion site (Fig. 8A). Thus, as previously described (Peters et al., 1991), the two adjacent membranes lie parallel to each other and converge to a nearly complete obliteration of the extracellular space (Fig. 8B).

Diverse combination of pre-embedding immunohistochemical protocols using DAB and gold particles for the visualization of different markers demonstrated the presence of gap junctions in GFP-identified implanted NPCs. Therefore, we found NPCs linked to other cellular elements through gap junctions (Fig. 8C; NPC labeled by GFP immunogold), which in some cases could be recognized as either other NPC profiles (Fig. 8D; both NPC processes identified by GFP immunogold) or presumptive astrocytes (Fig. 8E; NPC and gap junction labeled by GFP immunocytochemistry with DAB and Cx43 immunogold, respectively). Occasionally, gap junctions were also found between NPC and microglial processes (identified by GFP immunogold and Iba1 immunolabeling with DAB, respectively, Fig. 8I). Astrocytes joined together by gap junctions with Cx43 were also commonly observed (Fig. 8F; Cx43 immunogold). An interesting finding was that microglia cells also presented gap junctions, not only linked to NPCs (Fig. 8I), but also to other unidentified profiles (Fig. 8G,H).

Discussion

In this study we demonstrate that microglial activation after CNS injury can be regulated by implanted NPCs. In addition, we show evidence of Cx43 expression and the presence of gap junctions in implanted NPCs, reactive microglia and astrocytes at the lesion site, providing anatomical bases for gap junctional coupling between implanted NPCs and host glia.

It is well known that axon injury rapidly activates astroglial and microglial cells at the lesion site. Reactive astrocytes up-regulate GFAP and microglial cells proliferate, express inflammatory and immune mediators and acquire phagocytic activity upon activation (Aldskogius and Kozlova, 1998). The glial reaction to the transection of the MLF has been previously characterized (Pastor et al., 2000) and, as in other models of axotomy, a remarkable astrocytic and microglial activation is produced around the lesion. We now describe that the glial reaction to MLF transection was modified in animals receiving NPC implants. Thus, whereas GFAP immunoreactivity in the lesion site was similar in axotomized and NPC-implanted animals, OX-6 immunoreactivity in NPC-grafted animals significantly increased by twofold with respect to only injured animals. Therefore, the presence of NPCs in the host tissue induced an alteration in the microglial response to the lesion. Mosher et al. (2012) described that 24 h after NPC transplants in rat striatum, the microglial cell number was significantly increased in the site of grafting compared to animals that received only vehicle injections. In their study, all type of microglial cells (resting and activated) were identified by immunohistochemistry for the general microglial marker Iba1, although they also described an increased number of microglia with activated morphology in NPC-grafted animals compared to vehicle-injected ones. We have analyzed only the activated microglial population (immunoreactive to OX-6) at a much longer time period (two months), and still a considerable difference in microglial activation was quantified between implanted and axotomized animals. Therefore, we demonstrate that NPCs can up-regulate microglial activation *in vivo* after a mechanical brain lesion and this effect is maintained over time.

In line with this, our confocal analysis revealed a close association between grafted NPCs and activated microglial cells in the lesion environment. NPC processes were often located in intimate apposition to microglia and occasionally enwrapped a large extent of the microglial cell. This anatomical relationship probably indicates that both cell types can interact either directly, via gap junctions, or paracrinally, through the release of diffusible factors. For instance, Mosher et al. (2012) demonstrated a NPC-secreted factor involved in the regulation of host microglia, the vascular endothelial growth factor (VEGF). Interestingly, we have previously reported that postnatal SVZ-derived NPCs are immunoreactive to VEGF eight weeks after implantation (Talaverón et al., 2013), suggesting the possibility that this factor could also participate in the microglial response to NPC implants in our lesion model. Other authors have also described the importance of the interaction of implanted NPCs with microglia for the functional recovery from spinal cord injury induced by NPC grafting (Pluchino et al., 2005; Ziv et al., 2006). As it happened with microglia, a close proximity was also observed between host astrocytes and implanted NPCs, which also provides an anatomical basis for possible direct and/or paracrine communications between these two types of cells after injury.

Direct appositions between grafted NPCs and recipient astroglial and microglial cells were also confirmed at the ultrastructural level, so we next questioned the possibility of gap junctional communication among these cells. As an initial step, we evaluated whether the gap junction protein Cx43 was expressed by NPCs, before and after implantation, and also by glial cells surrounding the lesion. Before implantation,
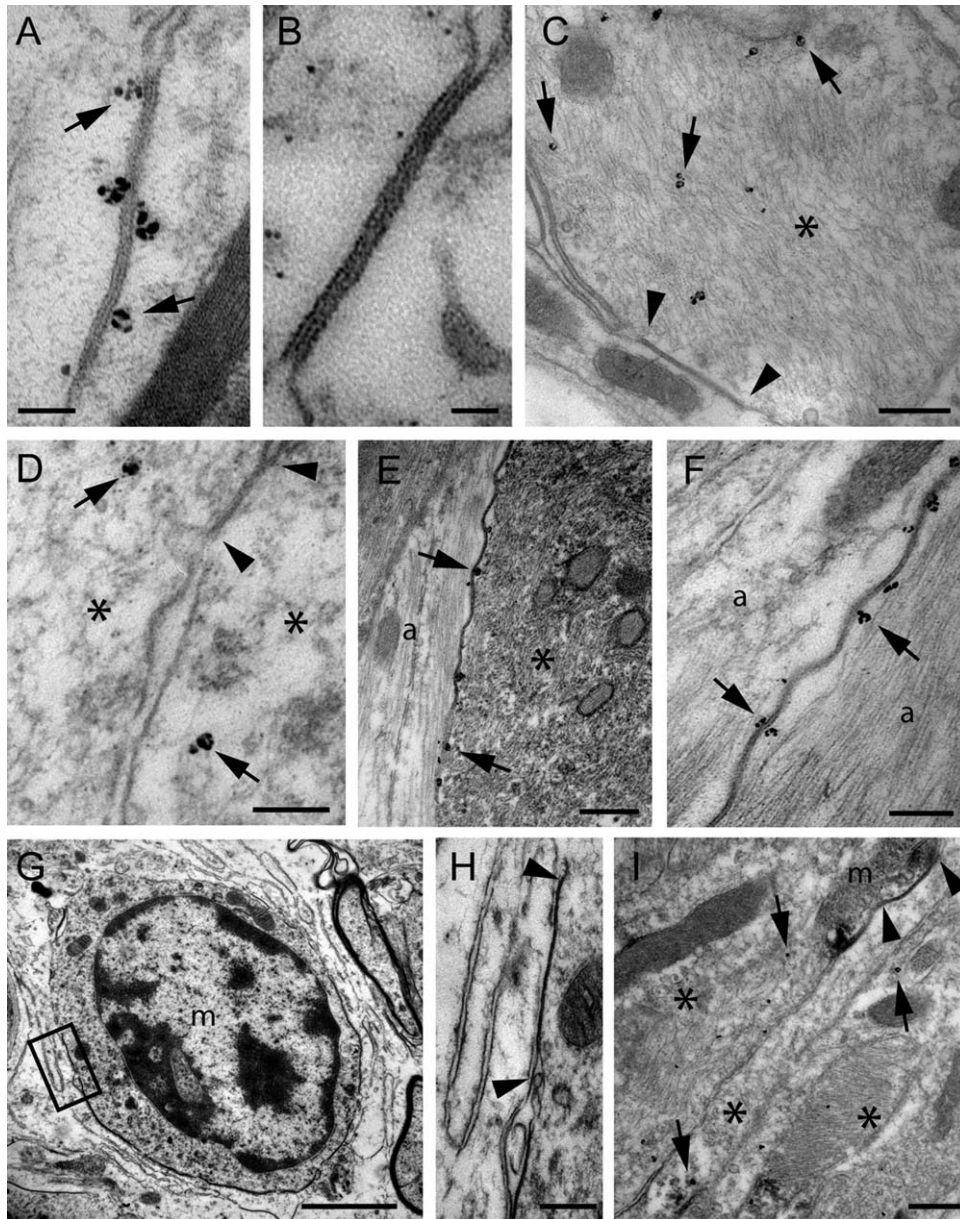
FIGURE 8: Electron microscopy images of gap junctions in implanted NPCs, astrocytes, or microglial cells at the lesion site. (A): Identification of gap junctions by Cx43 immunogold in pre-embedding. Note the gold particles (arrows) attached to the cell membranes at both sides of the junction. Scale bar = 0.1 μm. (B): Higher magnification of a gap junction showing the intimate apposition of the two cell membranes characteristic of this type of coupling, as well as the detachment of both membranes, and consequent widening of the extracellular space, at the edges of the junctional zone. Scale bar = 0.05 μm. (C): Example of a NPC process (asterisk) identified by pre-embedding immunogold against GFP (arrows point to some gold particles) linked to other cellular element by a gap junction (delimited between arrowheads). Scale bar = 1 μm. (D): Two different NPC elements (asterisks) identified by pre-embedding GFP immunogold (arrows point to gold particles) joined together by a gap junction (between arrowheads). Scale bar = 0.4 μm. (E): Electron microscopy image of an identified gap junction labeled by pre-embedding Cx43 immunogold in pre-embedding formed between a NPC (asterisk; identified by pre-embedding GFP immunocytochemistry with DAB) and a likely astrocyte (a). The gold particles (some of them indicated by arrows) denote the presence of the gap junction. Scale bar = 0.5 μm. (F): Pre-embedding Cx43 immunogold identification of a gap junction linking two presumptive astrocytes (a) as suggested by their typical filaments. Note the presence of gold particles (arrows), tagging the Cx43, at both sides of the junction. Scale bar = 0.2 μm. (G, H): Electron microscopy images of a putative microglial cell (m), suggested by its ultrastructural characteristics, coupled to another cellular element by a gap junction (framed region). H shows at a higher magnification the marked region in G to illustrate the gap junction between this likely microglia and another unidentified cellular process. Arrowheads delimit the junctional zone. Scale bars = G, 2 μm; H, 0.2 μm. (I): Three NPC processes (asterisks) identified by pre-embedding GFP immunogold (arrows point to some gold particles) and an identified DAB-labeled microglial element (m; after Iba1 pre-embedding immunocytochemistry), all of them in close apposition. Note the presence of a gap junction between one of the NPC elements and the microglia; arrowheads indicate the limits of this junction. Scale bar = 0.8 μm.

the analysis of Cx43 expression in cells from SVZ neurospheres revealed that the vast majority of the cells within each neurosphere presented Cx43 immunoreactivity and were neural progenitor cells, as revealed by nestin immunolabeling. These results are in agreement with others (Duval et al., 2002) that showed a high degree of Cx43 expression in undifferentiated cells from mouse embryonic striatal ventricular zone neurospheres suggesting an active role of Cx43 and intercellular communication during proliferation and differentiation of NPCs. Next, we analyzed Cx43 expression by NPCs eight weeks after their implantation. Most of the GFP-positive implanted NPCs were immunoreactive to Cx43 and remained in a nestin-expressing undifferentiated state. Other authors have reported that when NPCs are implanted in inflamed brain, a crosstalk between transplanted NPCs and immune cells is established that preserves the NPCs in a non-differentiated state (Pluchino et al., 2005) and that, in this state, they exert neuroprotective actions by immunomodulatory mechanisms (Pluchino et al., 2005; Ziv et al., 2006). Thus, it is possible that the inflammatory response associated to injury probably preserves the NPCs in a Cx43-expressing undifferentiated state in which they are able to communicate with each other and/or with host cells by gap junctions.

Host astrocytes at the lesion site also expressed Cx43 and formed gap junctions. Interestingly, in many of the astrocytes located adjacent to NPCs, Cx43 immunoreactive profiles were identified in the interface between the GFP-positive NPC and the astrocyte, a result confirmed by electron microscopy. Therefore, these findings indicate that NPCs can communicate with host astrocytes through gap junctions. With respect to microglia, our data showed the presence of Cx43 protein in activated OX-6 expressing microglia. Eugenin et al. (2001) previously demonstrated that, under resting conditions *in vivo*, most microglia do not express Cx43 but they do so at brain stab wounds. In this work, we describe Cx43 expression in activated microglia after a central fascicle transection, and it is important to highlight that some of these Cx43-immunoreactive profiles appeared located closely adjacent to implanted NPCs. Furthermore, gap junctions were demonstrated by electron microscopy in microglial cells and, occasionally, between an implanted NPC and a microglial cell identified by Iba1 immunolabeling.

Our findings suggest that implanted NPCs could communicate with recipient astroglial and microglial cells through gap junctions at a long time period after lesion. To our knowledge, this is the first study that demonstrates gap junctions between implanted NPCs and host glia *in vivo*, in adult animals, and at a long time after injury. In 2010, Jäderstad et al. reported gap junctional coupling between implanted NPCs and host neurons and the importance of such communication for the survival and protective actions attributed to the cell implants. NPCs were grafted in mutant murine models that underwent Purkinje neuron degeneration and they demonstrated that early cell coupling by gap junctions between grafted NPCs and host Purkinje neurons was essential to rescue these cerebellar neurons from degeneration. In our study, however, the lesion model was different (central axotomy) and evaluation of the presence of gap junctions was undertaken at the ultraestructural level and two months after the damage. Therefore, we suggest that not only paracrine signals can be established between implanted NPCs and host glia, but also direct communication through gap junctions, in which coupled cells can share small molecules, ions or some metabolites with an essential role in the neutralization of pathological processes, in the prevention from cell death, or in the improvement of neuronal function.

Conclusions

In summary, we have revealed an intimate association between implanted NPCs and host glial cells at the injury site in a model of central lesion. In particular, we have shown the ability of NPCs to up-regulate microglial reaction to injury after their implantation in the brain of adult animals suffering a mechanical damage. Furthermore, we have demonstrated the presence of gap junctions in implanted NPCs and host astrocytes and microglia. Our findings establish the possibility that, not only diffusible factors, but also cell-to-cell direct coupling might play an important role in graft-host communication with benefits for NPC integration in the tissue as well as for their neuroprotective effects following lesion.

References

Aldskogius A, Kozlova EN. 1998. Central neuron-glial and glial-glial interactions following axon injury. Prog Neurobiol 55:1–26.

Alvarez-Buylla A, Seri B, Doetsch F. 2002. Identification of neural stem cells in the adult vertebrate brain. Brain Res Bull 57:751–758.

Anderson DJ. 2001. Stem cells and pattern formation in the nervous system: The possible *versus* the actual. Neuron 30:19–35.

Bruzzone R, White TH, Paul DL. 1996. Connection with connexins: The molecular basis of direct intercellular signaling. Eur J Biochem 238:1–27.

Carpenter MK, Cui K, Hu ZY, Jackson J, Sherman S, Seiger A, Wahlberg LU. 1999. *In vitro* expansion of a multipotent population of human neural progenitor cells. Exp Neurol 158:265–278.

Cheng A, Tang J, Cai J, Zhu M, Zhang X, Rao M, Mattson MP. 2004. Gap junctional communication is required to maintain mouse cortical neural progenitor cells in a proliferative state. Dev Biol 272:203–216.

Chew SSL, Johnson CS, Gree CR, Danesh-Meyer HV. 2010. Role of connexin43 in central nervous system injury. Exp Neurol 225:250–261.

Contreras JE, Sanchez HA, Veliz LP, Bukauskas FF, Bennet MV, Sáez JC. 2004. Role of connexin-based gap junction channels and hemichannels in ischemia induced cell death in nervous system. Brain Res Rev 47:290–303.

Cummings BJ, Uchida N, Tamaki SJ, Salazar DL, Hooshmand CN, Summers R, Gage FH, Anderson AJ. 2005. Human neural stem cells differentiate and promote locomotor recovery in spinal cord-injured mice. Proc Natl Acad Sci USA 102:14069–14074.

Danscher G, Zimmer J. 1978. An improved Timm-sulphide method for light and electron microscopic localization of heavy metals in biological tissues. Histochemistry 55:27–40.

de la Cruz RR, Delgado-García JM, Pastor AM. 2000. Discharge characteristics of axotomized abducens internuclear neurons in the adult cat. J Comp Neurol 427:391–404.

Duval N, Gomès D, Calaora V, Calabrese A, Meda P, Bruzzone R. 2002. Cell coupling and Cx43 expression in embryonic mouse neural progenitor cells. J Cell Sci 16:3241–3251.

Elias LAB, Wang DD, Kriegstein AR. 2007. Gap junction adhesion is necessary for radial migration in the neocortex. Nature 448:901–907.

Englund U, Bjorklund A, Wictorin K, Lindvall O, Kokaia M. 2002. Grafted neural stem cells develop into functional pyramidal neurons and integrate into host cortical circuitry. Proc Natl Acad Sci USA 99:17089–17094.

Esen N, Shuffield D, Syed MM, Kielian T. 2007. Modulation of connexin expression and gap junction communication in astrocytes by the gram-positive bacterium *S. Aureus*. Glia 55:104–117.

Eugenin EA, Eckardt D, Theis M, Willecke K, Bennet MV, Sáez JC. 2001. Microglia at brain stab wounds express connexin43 and *in vitro* form functional gap junctions after treatment with interferon-γ and tumor necrosis factor-α. Proc Natl Acad Sci USA 7:4190–4195.

Gage FH. 2000. Mammalian neural stem cells. Science 287:1433–1438.

Garg S, Syed MM, Kielian T. 2005. *Staphylococcus aureus*-derived peptidoglycan induces Cx43 expression and functional gap junction intercellular communication in microglia. J Neurochem 95:475–483.

Jäderstad J, Jädersatd LM, Li J, Chintawar S, Salto C, Pandolfo M, Ourednik V, Teng YD, Sidman RL, Arenas E, Snyder EY, Herlenius E. 2010. Communication via gap junctions underlies early functional and beneficial interactions between grafted neural stem cells and the host. Proc Natl Acad Sci USA 11:5184–5189.

Jeong SW, Chu K, Jung KH, Kim SU, Kim M, Roh JK. 2003. Human neural stem cell transplantation promotes functional recovery in rats with experimental intracerebral hemorrhage. Stroke 34:2258–2263.

Kelly S, Bliss TM, Shah AK, Sun GH, Ma M, Foo WC, Masel J, Yenari MA, Weissman IL, Uchida N, Palmer T, Steinberg GK. 2004.Transplanted human fetal neural stem cells survive, migrate and differentiate in ischemic rat cerebral cortex. Proc Natl Acad Sci USA 101:11839–11844.

Kumar NM, Gilula NB. 1996. The gap junction communication channel. Cell 84:381–388.

Lacar B, Young SZ, Platel JC, Bordey A. 2011. Gap junction-mediated calcium waves define coomunication networks among murine postnatal neural progenitor cells. Eur J Neurosci 34:1895–1905.

Lee I-H, Lindqvist E, Kiehn O, Widenfalk J, Olson L. 2005. Glial and neuronal connexin expression patterns in the rat spinal cord during development and following injury. J Comp Neurol 489:1–10.

Macías D, Oya R, Saniger L, Martín F, Luque F. 2009. A lentiviral vector that activates latent human immunodeficiency virus-1 proviruses by the overex-

pression of tat and that kills the infected cells. Hum Gene Ther 20:1259–1268.

Marins M, Xavier ALR, Viana NB, Fortes FS, Fróes MM, Menezes JR. 2009. Gap junctions are involved in cell migration in the early postnatal subventricular zone. Dev Neurobiol 69:715–730.

McBride JL, Behrstock SP, Chen EY, Jakel RJ, Siegel I, Svendsen CN, Kordower JH. 2004. Human neural stem cell transplants improve motor function in a rat model of Huntington's disease. J Comp Neurol 475:211–219.

Miragall F, Albiez P, Bartels H, de Vries U, Dermietzel R. 1997. Expression of the gap junction protein connexin43 in the subependymal layer and the rostral migratory stream of the mouse: Evidence for an inverse correlation between intensity of connexin43 expression and cell proliferation activity. Cell Tissue Res 287:243–253.

Morado-Díaz CJ, Matarredona ER, Davis-López de Carrizosa MA, de la Cruz RR, Pastor AM. 2011. Neural progenitor cell implants in the lesioned medial longitudinal fascicle of adult cats regulate synaptic composition of abducens internuclear neurons. Soc Neurosci Meet Abstr 438:17.

Mosher KI, Andres RH, Fukuhara T, Bieri G, Hasegawa-Moriyama M, He Y, Guzman R, Wyss-Coray T. 2012. Neural progenitor cells regulate microglia functions and activity. Nat Neurosci 15:1485–1487.

Nagy JI, Rash JE. 2000. Connexins and gap junctions of astrocytes and oligodendrocytes in the CNS. Brain Res Rev 32:29–34.

Nakase T, Yoshida Y, Nagata K. 2006. Enhanced connexin43 immunoreactivity in penumbral areas in the human brain following ischemia. Glia 54:369–375.

Pastor AM, Delgado-García JM, Martínez-Guijarro FJ, López-García C, de la Cruz RR. 2000. Response of abducens internuclear neurons to axotomy in the adult cat. J Comp Neurol 427:370–390.

Paxinos G, Watson C. 1997. The rat brain in stereotaxic coordinates. New York: Academic Press.

Peters A, Palay SL, Webster HD. 1991. The Fine Structure of the Nervous System: Neurons and their Supporting Cells, 3rd ed. New York, NY: Oxford University Press.

Pluchino S, Quattrini A, Brambilla E, Gritti A, Salani G, Dina G, Galli R, DelCarro U, Amadio S, Bergami A, Furlan R, Comi G, Vescovi AL, Martino G. 2003. Injection of adult neurospheres induces recovery in a chronic model of multiple sclerosis. Nature 422:688–694.

Pluchino S, Zanotti L, Rossi B, Brambilla E, Ottoboni L, Salani G, Martinello M, Cattalini A, Bergami A, Furlan R, Comi G, Constantin G, Martino G. 2005. Neurosphere-derived multipotent precursors promote neuroprotection by an immunomodulatory mechanism. Nature 436:266–271.

Pluchino S, Cossetti C. 2013. How stem cells speak with host immune cells in inflammatory brain diseases. Glia 61:1379–1401.

Rash JE, Yasumura T, Davidson KGV, Furman CS, Dudek FE, Nagy JI. 2001. Identification of cells expressing Cx43, Cx30, Cx26, Cx32 and Cx36 in gap junctions of rat brain and spinal cord. Cell Commun Adhes 8:315–320.

Reynolds BA, Weiss S. 1992. Generation of neurons and astrocytes from isolated cells of the adult mammalian central nervous system. Science 255:1707–1710.

Richardson RM, Broaddus WC, Holloway KL, Fillmore HL. 2005. Grafts of adult subependymal zone neuronal progenitor cells rescue hemiparkinsonian behavioural decline. Brain Res 1032:11–22.

Santiago MF, Alcami P, Striedinger KM, Spray DC, Scemes E. 2010. The carboxyl-terminal domain of Connexin43 is a negative regulator of neuronal differentiation. J Biol Chem 285:11836–11845.

Söhl G, Willecke K. 2003. An update on connexin genes and their nomenclature in mouse and man. Cell Commun Adhes 10:173–180.

Svendsen CN, Clarke DJ, Rosser AE, Dunnet SB. 1996. Survival and differentiation of rat and human epidermal growth factor-responsive precursor cells following grafting into the lesioned adult central nervous system. Exp Neurol 137:376–388.

Talaverón R, Matarredona ER, de la Cruz RR, Pastor AM. 2013. Neural progenitor cell implants modulate vascular endothelial growth factor and brain-derived neurotrophic factor expression in rat axotomized neurons. PLoS One 8:e54519.

Torroglosa A, Murillo-Carretero M, Romero-Grimaldi C, Matarredona ER, Campos-Caro A, Estrada C. 2007. Nitric oxide decreases subventricular zone stem cell proliferation by inhibition of epidermal growth factor receptor and phosphoinositide-3-kinase/Akt pathway. Stem Cells 25:88–97.

Whitman MC, Fan L, Rela L, Rodriguez-Gil DJ, Greer CA. 2009. Blood vessels form a migratory scaffold in the rostral migratory stream. J Comp Neurol 516:94–104.

Yang M, Stull ND, Berk MA, Snyder EY, Iacovitti L. 2002. Neural stem cells spontaneously express dopaminergic traits after transplantation into the intact or 6-hydroxydopamine-lesioned rat. Exp Neurol 177:50–60.

Ziv Y, Avidan H, Pluchino S, Martino G, Schwartz M. 2006. Synergy between immune cells and adult neural stem/progenitor cells promotes functional recovery from spinal cord injury. Proc Natl Acad Sci USA 103: 13174–13179.